From a feedback-controlled demon to an information ratchet in a double quantum dot

Debankur Bhattacharyya [1,*] and Christopher Jarzynski [2,†]

[1] *Institute for Physical Science and Technology, University of Maryland, College Park, Maryland 20742, USA*

[2] *Institute for Physical Science and Technology, Department of Chemistry and Biochemistry, and Department of Physics, University of Maryland, College Park, Maryland 20742, USA*

(Received 5 June 2022; accepted 15 November 2022; published 2 December 2022)

We present a simple strategy for constructing an information ratchet or memory-tape model of Maxwell's demon, from a feedback-controlled model. We illustrate our approach by converting the Annby-Andersson feedback-controlled double quantum dot model [Phys. Rev. B **101**, 165404 (2020)] to a memory-tape model. We use the underlying network structure of the original model to design a set of bit interaction rules for the information ratchet. The new model is solved analytically in the limit of long interaction times. For finite-time interactions, semianalytical phase diagrams of operational modes are obtained. Stochastic simulations are used to verify theoretical results.

DOI: 10.1103/PhysRevE.106.064101

I. INTRODUCTION

In a letter to Peter Tait in 1867, James Maxwell described a thought experiment in which a hypothetical creature—now known as Maxwell's demon—seemingly beats the second law of thermodynamics by performing measurements and feedback on the motions of individual gas molecules. This thought experiment initiated a line of research that exposed deep connections between thermodynamics and information processing. Recent years have seen renewed activity in this field, with theoretical progress as well as experimental studies adding to our understanding of these connections. See, for example, Ref. [1] for a review of the history of Maxwell's demon and the current experimental state of the art and Ref. [2] for an introduction to the theoretical formalism of information thermodynamics.

Over the past century and a half, numerous variations of Maxwell's demon have been proposed, notably including Smoluchowski's trapdoor [3–5], Szilard's engine [6], and Feynman's ratchet and pawl [7,8] as early examples. These and other demons can broadly be classified according to two paradigms: feedback-controlled demons and autonomous demons. In the feedback-controlled paradigm, exemplified by both Maxwell's thought experiment and Szilard's engine, the demon is an external agent who performs measurements and provides feedback based on the outcomes of those measurements. The physical nature of the demon is unspecified and irrelevant. Recent stochastic-thermodynamic analyses of feedback-controlled demons have led to the discovery of inequalities and fluctuation relations that sharpen our understanding of information thermodynamics. [9–18]

In the autonomous paradigm, by contrast, the demon is a physical device that is cleverly designed to achieve, through the rectification of thermal noise, the same outcome that a feedback-controlled demon achieves through measurements and feedback. Smoluchowski's trapdoor and Feynman's ratchet and pawl are examples of autonomous demons that at first glance appear to bring about their intended outcomes, but upon closer inspection are seen to fail. These examples are often held up as cautionary tales highlighting the futility of trying to invent a gadget that defies the second law of thermodynamics. Bennett, however, argued that an autonomous demon could succeed if it were coupled to a memory storage device [19–21]. Due to the physical nature of information, as proposed by Landauer [22,23], these models of autonomous demons can utilize the memory storage device as an *information reservoir* [24] to mimic the same functionality as feedback-controlled models of Maxwell's demon. In these models, the decrease of environmental entropy is compensated by an increase in the randomness of the informational state of the memory storage device. Often these models of autonomous Maxwell's demons or *information ratchets* are visualized by imagining a system that interacts with a sliding memory tape containing a sequence of bits (the information reservoir) and are called *memory-tape models*.

Mandal and Jarzynski (MJ) introduced an explicit stochastic model of a memory-tape autonomous demon [25] and similar models have been developed for both classical and quantum systems [26–40]. Memory-tape models have recently been studied as *transducers* from the computer science and information theory perspective and the thermodynamic implications of correlation among the bits of the memory-tape have been discussed [41–49]. *Repeated interaction models*, commonly used in quantum thermodynamics, have also been used to discuss the thermodynamics of the memory-tape models [50]. Autonomous demons can also be driven by temperature differences; see Refs. [51,52] and references therein, but in the present work we focus on autonomous models driven by information reservoirs.

*dbhattac@umd.edu

†cjarzyns@umd.edu

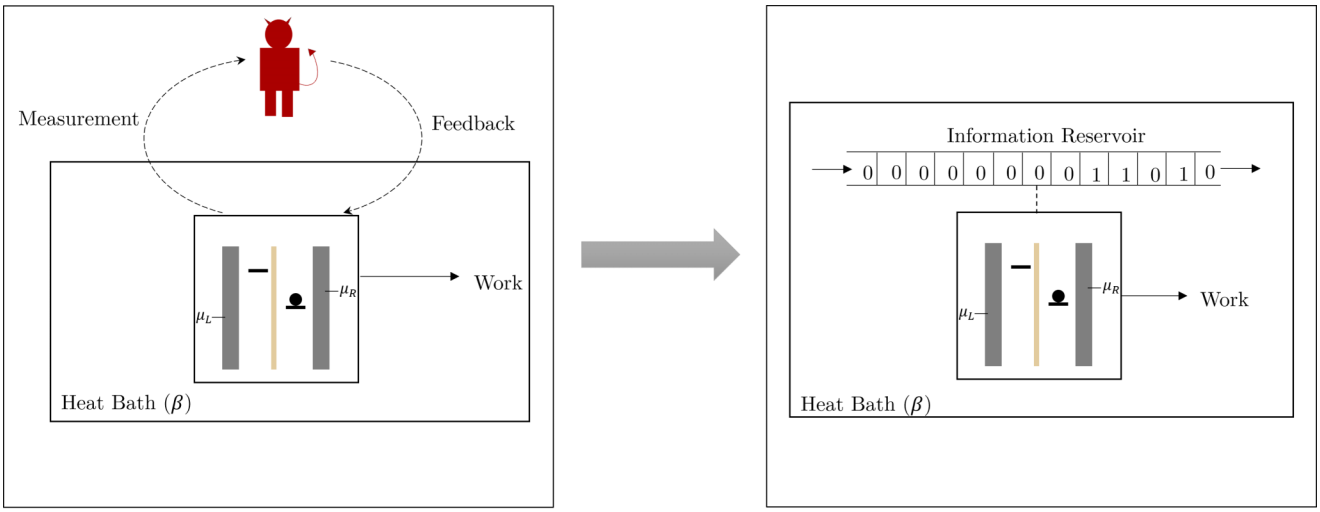

Feedback-controlled model of Maxwell's demon in DQD (AA Model)

Memory-tape model of Maxwell's demon in DQD

FIG. 1. Two paradigms of Maxwell's demon. The left figure depicts the AA model—a feedback-controlled model. On the right we show the corresponding memory-tape model or information ratchet. In both cases, heat from a thermal reservoir is converted to work, either through measurement and feedback, or through interaction with an information reservoir. We explore a strategy to convert a feedback-controlled model to a memory-tape model.

A number of authors have explored connections between feedback-controlled and memory-tape models [30,36,53–55]. Horowitz *et al.* [53] designed a feedback-controlled information motor based on the system-bit interactions of Ref [25]. Barato and Seifert [30,31] discussed a stochastic thermodynamics [16] framework that encompasses both feedback-controlled and memory-tape models. Shiraishi *et al.* [55] showed that the measurement-feedback model introduced in Ref. [53] can be reduced to the simplified MJ model of Refs. [29–31]. Strasberg *et al.* [36] described a system with a spin-valve and a quantum dot that can mimic the thermodynamic behavior of the MJ model and can be mapped to a Brownian ratchet. They also presented a feedback-controlled model that captures the effective dynamics of the corresponding memory-tape model and they compared how the second law of thermodynamics applies to these two paradigms.

In this article we use a recently introduced model [56] to develop and illustrate a general strategy for converting a nonautonomous, feedback-controlled model of Maxwell's demon into an autonomous, memory-tape model or information ratchet as illustrated schematically in Fig. 1. Our approach uses network based modeling [16,57] of a system of master equations, originally introduced by Schnakenberg in Ref. [58], to show how a nonautonomous demon with a seemingly complicated feedback protocol can systematically be modified to construct a memory-tape model that mimics its behavior. We illustrate this strategy by applying it to the recently proposed *Annby-Andersson* (AA) model [56] of a double quantum dot (DQD) [59,60]. We then present a theoretical analysis of the resulting memory-tape model. Our model has distinct regions in parameter space where it operates either as an *information engine* or as a *Landauer eraser*. We solve the model exactly in the limit when each bit interacts with the DQD for an infinite amount of time, obtaining analytic expressions for thermodynamic quantities and critical parameter values. We also semianalytically explore the finite time bit-interaction situation and show the corresponding phase diagrams. Lastly, we discuss a scheme for the stochastic simulation of memory-tape models and use it to simulate our model to verify the semianalytical results. We limit our discussion to a completely classical stochastic model and leave quantum models as a future avenue for research.

This article is organized as follows. In Sec. II, we briefly review the Annby-Andersson model [56], which is the starting point for designing our memory-tape model. Details of network based stochastic modeling [16,57,58] are presented in Sec. III. In Sec III A we map the AA model to a nine-state network by converting its control parameter to a stochastic variable. In Sec. III B and Sec. III C, we discuss how to couple the DQD with incoming bits to mimic the behavior of the feedback-controlled demon. A summary of the general modeling scheme is presented in Sec. III D. The analysis of memory-tape models is discussed in Sec. IV A. In Sec. IV B we discuss the thermodynamics of our model and solve for analytical expressions of thermodynamic quantities in Sec. IV C. Phase diagrams of operational modes are discussed in Sec. IV D and the stochastic simulation scheme for the model is presented in Sec. IV E.

II. BACKGROUND AND SETUP: ANNBY-ANDERSSON MODEL

A quantum dot (QD) is an artificial nanoscale structure for confining electrons. Since it is possible to tune the energetic cost of adding an excess electron, QDs act as "artificial atoms" with tunable energy levels [59–61]. The charge state of a single-level quantum dot can be labeled as either empty

or occupied based on the absence or presence of the excess electron. The system in the AA model consists of two coupled QDs, each connected to an electron reservoir maintained at a fixed chemical potential ($\mu_{L/R}$) and temperature T; see Ref. [56]. The energy level of each dot can be tuned to three possible values ϵ_l, ϵ_0, and ϵ_u, with $\epsilon_l < \epsilon_0 < \epsilon_u$. Coulomb repulsion prevents the DQD from being occupied by more than a single excess electron. Hence the possible *occupation states* are (i) L, the left dot contains the excess electron, (ii) R, the right dot contains the excess electron, and (iii) E, both dots are unoccupied. The charge state of the DQD is monitored continuously and a feedback scheme is applied. The electron reservoirs coupled to the left and right dots are maintained at chemical potentials μ_L and μ_R. If $\mu_R > \mu_L$, transferring an electron from the left to the right reservoir requires electrical work to be performed against a voltage bias.

The protocol of the AA model [56] was originally introduced in Ref. [62]. In the ideal mode of operation the DQD starts in the empty state, with the energy level of the left dot at ϵ_0 and that of the right dot at ϵ_u, where $(\epsilon_u - \mu_{L/R}) \gg k_B T$ and k_B is Boltzmann's constant. When (a) an electron enters the left dot from the left reservoir, (b) instant feedback is applied to change the energy levels of both the left and right dots to ϵ_l, where $(\mu_{L/R} - \epsilon_l) \gg k_B T$. During this first feedback step, the external agent extracts $(\epsilon_0 - \epsilon_l)$ work. Next, the system is monitored until (c) the electron tunnels from the left to the right dot, at which point (d) feedback is applied to change the energy level of the left dot to ϵ_u and the right dot to ϵ_0. The external agent performs $(\epsilon_0 - \epsilon_l)$ work during this second feedback step, canceling the work extraction of the previous step. Finally, (e) when the electron jumps from the right dot to the right reservoir, (f) feedback is applied again to switch the energy levels of the DQD back to their initial values. No work is performed during this step, as the DQD is empty. This three-step cyclic protocol transfers an electron from the left to the right reservoir. Since no net work is performed by the external agent, the energy for this transfer must come from the thermal reservoirs. Thus the feedback-driven cycle ultimately converts heat into chemical work, of the amount $W_{\text{ext}} = (\mu_R - \mu_L)$; see Ref. [56] for more details. The protocol discussed above is shown in Fig. 2, where electron transition events are indicated by single arrows and feedback steps by double arrows. The labels of the arrows in Fig. 2 refer to the steps of the protocol mentioned above. The states in Fig. 2 that are not included in the ideal protocol for the AA model are relevant for the memory tape model, which is discussed later in this article.

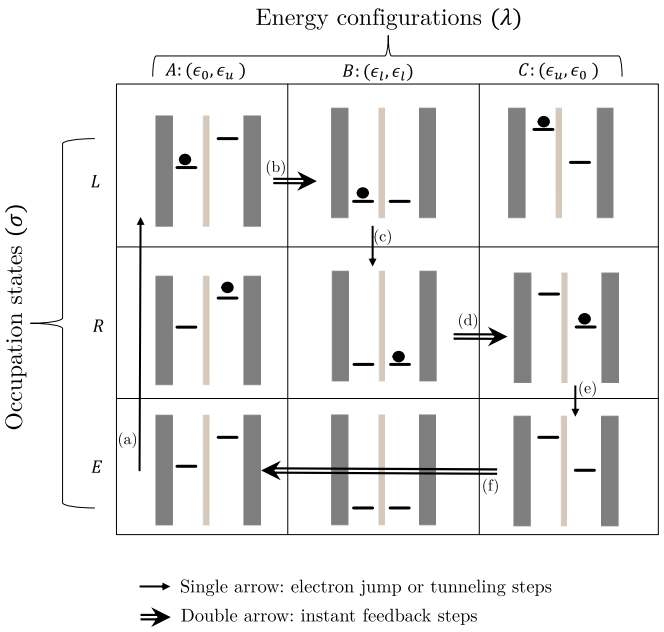

FIG. 2. States of the double quantum dot system $x \equiv (\lambda, \sigma)$ and the protocol ($\mathcal{C}_{AA}$) for the AA model. Feedback steps [changes in λ, i.e., steps (b), (d), and (f)] are shown using double arrows and electron jumps [changes in σ, i.e., steps (a), (c), and(e)] are shown using a single arrow.

III. MEMORY-TAPE MODEL OF MAXWELL'S DEMON IN DQD SYSTEM

A. Reduced network: Nine states

1. Network structure

We now construct a network representation of the states of the AA model, as a first step toward designing a corresponding memory-tape model. In the AA model, the DQD occupation state σ is a dynamic variable with three possible states, $\sigma \in \mathbf{\Sigma} = \{L, E, R\}$, as described above. The DQD *energy configuration* λ acts as a control parameter, also with three possible states: $\lambda \in \mathbf{\Lambda} = \{A, B, C\}$, where $A \equiv (\epsilon_0, \epsilon_u)$, $B \equiv (\epsilon_l, \epsilon_l)$, and $C \equiv (\epsilon_u, \epsilon_0)$. Combining the energy configurations and the occupation states leads to nine possible states for the *DQD state variable*: $x \in \mathbf{V_x} = \mathbf{\Lambda} \times \mathbf{\Sigma} = \{AL, AE, \ldots, CR\}$. The ideal cyclic protocol $\mathcal{C}_{AA}$, described above, follows the path $AE \longrightarrow AL \Rightarrow BL \longrightarrow BR \Rightarrow CR \longrightarrow CE \Rightarrow AE$, where double arrows signify feedback steps; see Fig. 2.

We now consider a situation in which the energy configuration λ is no longer a control parameter, but instead is a dynamical variable on the same footing as the occupation state σ. In our model, the entire system is maintained at a temperature T using a thermal bath and λ is now a stochastic variable that evolves under the effect of the thermal noise from the bath. The system-variable $x \equiv (\lambda, \sigma)$ evolves among the nine states in $\mathbf{V_x}$ as a continuous time Markov jump process. We justify the Markov assumption by assuming that the system-bath coupling is weak and that the correlation of the system with the bath dies in a faster timescale than the timescale of the jumps. We make the following assumptions about our model. (i) The elementary transitions in our process involve a change in either λ, or σ, but not both simultaneously, i.e., the system is *bipartite* [57]. (ii) If $\lambda = B$, then the excess electron cannot hop into or out of the electron reservoirs; thus the transitions $BE \leftrightarrow BL$ and $BE \leftrightarrow BR$ are not allowed. (iii) Direct transitions between A and C states are forbidden. These assumptions are modeling choices, but we note that all of the forbidden transitions can be justified physically by assuming sufficiently high energy barriers between corresponding states.

Under these assumptions, we obtain a network $\mathcal{G}_r = (\mathbf{V_x}, \mathbf{E_x})$, where $\mathbf{V_x} \equiv V(\mathcal{G}_r)$ is the set of nine vertices and $\mathbf{E_x} \equiv E(\mathcal{G}_r)$ is the set of 11 bidirectional edges (see Fig. 3)

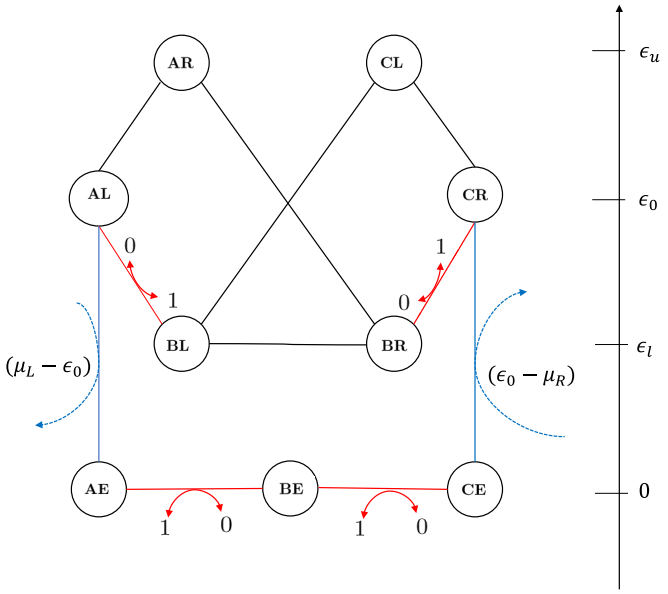

FIG. 3. Reduced network $\mathcal{G}_r = (\mathbf{V_x}, \mathbf{E_x})$. Energies of the states in $\mathbf{V_x}$ are shown to the right of the network. Edges shown in red correspond to the feedback steps of the original AA model and involve the flipping of the bit in the memory-tape model. The edges shown in blue correspond to the transitions where the electron hops into (out of) the DQD from (to) an electron reservoir and the dotted arrows show the corresponding energy exchange.

describing the stochastic dynamics [16,57,58] of the variable $x \equiv (\lambda, \sigma)$. The subscript r in $\mathcal{G}_r$ indicates a *reduced* nine-state network, in contrast with a *full* 18-state network $\mathcal{G}_f$ to be defined later. As the control parameter λ is now converted to a stochastic variable which evolves under the thermal noise, the state $x \equiv (\lambda, \sigma)$ will not in general follow the protocol $\mathcal{C}_{AA}$ and is free to explore all the states in the network $\mathcal{G}_r$.

2. *Dynamics in the reduced network*

We set the energies of the empty states AE, BE, CE to zero and assign energies to all other states based on the energy level of the dot that contains the electron: states BL and BR have energy ϵ_l, states AL and CR have energy ϵ_0, and states AR and CL have energy ϵ_u, with $\epsilon_l < \epsilon_0 < \epsilon_u$ as mentioned earlier. We impose the condition of local detailed balance on the transition rates for the thermal transitions $x_i \leftrightarrow x_j$ with $x_i, x_j \in V(\mathcal{G}_r)$, when there is no exchange of electron with the left or the right reservoir:

$$\frac{R^r_{x_i x_j}}{R^r_{x_j x_i}} = e^{-\beta\left(E^r_i - E^r_j\right)}, \tag{1}$$

where $\beta = (k_B T)^{-1}$ is the inverse temperature and the superscript r again refers to the reduced network. E^r_i (E^r_j) is the energy of the state x_i (x_j) and $R^r_{x_i x_j}$ is the transition rate for the jump $x_j \to x_i$. The right-hand side of Eq. (1) is the ratio of probabilities of the system being in states x_i and x_j, when in canonical ensemble. Strictly speaking, the DQD system is quantum in nature and the tunneling events of the excess electron between two dots (i.e., $\sigma = L \leftrightarrow \sigma = R$) are coherent transfers, a purely quantum phenomenon. However, for our model we treat these events as classical thermal jumps for simplicity in the spirit of Ref. [56] as discussed in Sec. II. Thus we assume the local detailed balance relation Eq. (1) for the edges: $AL \leftrightarrow AR$, $BL \leftrightarrow BR$, and $CL \leftrightarrow CR$.

When an electron jumps from the right reservoir, maintained at the chemical potential μ_R, to the energy level ϵ_0 of the right dot, there is an energy cost of $(\epsilon_0 - \mu_R)$ and similarly if an electron jumps from the level ϵ_0 of the left dot to the left electron reservoir set at the chemical potential μ_L the energy exchange is $(\mu_L - \epsilon_0)$. Thus for the transitions $AL \leftrightarrow AE$ and $CR \leftrightarrow CE$ (shown in blue in Fig. 3), we can write the local detailed balance relations as

$$\frac{R^r_{AE\ AL}}{R^r_{AL\ AE}} = e^{-\beta(\mu_L - \epsilon_0)}, \quad \frac{R^r_{CR\ CE}}{R^r_{CE\ CR}} = e^{-\beta(\epsilon_0 - \mu_R)}. \tag{2}$$

The coupling with the electron reservoir creates *thermodynamic forces* [16,58,63,64] in $\mathcal{G}_r$ and leads to violation of global detailed balance when $\mu_L \neq \mu_R$. When Eqs. (1) and (2) are satisfied and $\mu_L \neq \mu_R$, the dynamics of x in $\mathcal{G}_r$ reach a nonequilibrium steady state (NESS) [16]. In this state, electrons flow in the thermodynamically preferred direction, i.e., from the right (left) reservoir to the left (right) reservoir when $\mu_R > \mu_L$ ($\mu_L > \mu_R$), resulting in an overall counterclockwise (clockwise) flow [which we will abbreviate as CCW (CW) flow throughout the article] of probability current in $\mathcal{G}_r$. This flow is in contrast with the feedback-controlled model, which transfers electrons against the thermodynamically preferred direction. Therefore, we next consider how to couple the DQD to an information reservoir, in the form of a stream of bits, so as to make the evolution of the DQD mimic that of the AA model.

B. Bit coupling strategy

Our information reservoir is a memory tape containing n classical bits. Each bit (b) can be in one of the two states in $\mathbf{B} = \{0, 1\}$. The energies of the two bit states are degenerate and we set them to zero. As in Ref. [25] the DQD interacts with a bit for an interval of duration τ, after which the next bit arrives. We can visualize this process by imagining that the bits are placed, equally spaced, on a tape that moves frictionlessly past the DQD, which interacts with the bit that is nearest to it at any given time.

In our model the coupling between the DQD and the bit occurs along the four edges of $\mathcal{G}_r$ that correspond to instant feedback steps in the AA model. These edges are shown in red in Fig. 3. (Note that we have split the $CE \Rightarrow AE$ feedback step of the original AA model into two steps: $CE \leftrightarrow BE$ and $BE \leftrightarrow AE$ in our model.) Specifically, the DQD transitions corresponding to these four edges can occur only when the state of the interacting bit b also flips. We set up the coupling rules so that the CW flow of probability current along $\mathcal{C}_{AA}$ is favored when b flips from 0 to 1 and CCW flow is favored when b flips from 1 to 0. For example, the transition $AL \to BL$ must be accompanied by a bit flip $0 \to 1$ and the reverse transition $BL \to AL$ occurs only if the interacting bit flips from 1 to 0. Similar comments apply to the edges $BR \leftrightarrow CR$, $CE \leftrightarrow BE$, and $BE \leftrightarrow AE$. These DQD-bit coupling rules are indicated by curved red arrows in Fig. 3. With this coupling scheme, an excess of 0's in the incoming bit stream biases the flow of probability in the CW direction. This

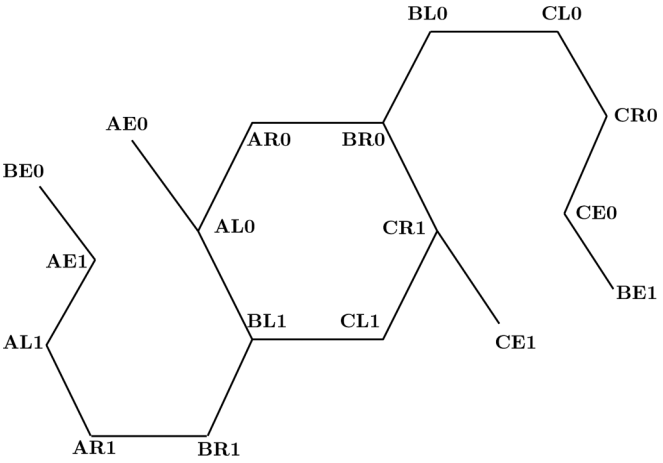

FIG. 4. Full network $\mathcal{G}_f = (\mathbf{V_y}, \mathbf{E_y})$ showing all 18 states of the combined DQD and bit. The full network $\mathcal{G}_f$ can be obtained from Fig. 3 by noticing the bit coupling in $\mathcal{G}_r$. The states in the full network are given by $\mathbf{V_y} = \mathbf{V_x} \times \mathbf{B}$ and the edges follow directly from the edges of the network $\mathcal{G}_r$; the mapping of the edges is described in Sec. III C 1. Equation (6) governs the dynamics of the variable $y \equiv (\lambda, \sigma, b)$ in this network.

bias opposes the thermodynamic direction of the probability current when $\mu_R > \mu_L$. Similarly, if $\mu_L > \mu_R$, then an excess of 1's opposes the thermodynamic direction of the probability current.

C. Full network: 18 states

1. Network structure

The joint evolution of the DQD state (x) and the nearest bit (b) occurs in the *bit-coupled network* $\mathcal{G}_f = (\mathbf{V_y}, \mathbf{E_y})$, which we refer to as the *full network*; see Fig. 4. Here $\mathbf{V_y} \equiv V(\mathcal{G}_f) = \mathbf{V_x} \times \mathbf{B}$ is the set of vertices representing the 18 possible states of the variable $y = (x, b) \equiv (\lambda, \sigma, b)$ and $\mathbf{E_y} \equiv E(\mathcal{G}_f)$ is the set of 18 bidirectional edges that reflect on the bit-coupling rules described in Sec. III B. Each edge of $\mathcal{G}_r$ that does not involve bit coupling is represented by two different edges of $\mathcal{G}_f$, corresponding to the two possible bit states. That is, an edge $x_i \leftrightarrow x_j \in E(\mathcal{G}_r)$ corresponds to the edges $(x_i, 0) \leftrightarrow (x_j, 0)$ and $(x_i, 1) \leftrightarrow (x_j, 1)$ in $E(\mathcal{G}_f)$, when $x_i \leftrightarrow x_j$ does not involve bit coupling. An edge $x_i' \leftrightarrow x_j' \in E(\mathcal{G}_r)$ that is coupled to the bit transition $0 \leftrightarrow 1$ is mapped to only one edge $(x_i', 0) \leftrightarrow (x_j', 1) \in E(\mathcal{G}_f)$. There are four such edges in $\mathcal{G}_f$: $BE0 \leftrightarrow AE1$, $AL0 \leftrightarrow BL1$, $BR0 \leftrightarrow CR1$, and $CE0 \leftrightarrow BE1$; see Figs. 3 and 4.

2. Dynamics in the full network

As the $b = 0$ and 1 bit states are energetically degenerate, the transition rates for the edges in $E(\mathcal{G}_f)$ obey the same detailed balance conditions as the corresponding edges in $E(\mathcal{G}_r)$. Edges $y_i \leftrightarrow y_j$ in $E(\mathcal{G}_f)$ with no electron reservoir coupling satisfy

$$\frac{R_{y_i y_j}}{R_{y_j y_i}} = e^{-\beta(E_i - E_j)}, \tag{3}$$

where E_i and E_j are the energies of the states y_i and y_j, respectively [compare Eq. (3) with Eq. (1)]. When there is a coupling with the electron reservoirs, the local detailed balance relations are given as

$$\frac{R_{AE0\,AL0}}{R_{AL0\,AE0}} = \frac{R_{AE1\,AL1}}{R_{AL1\,AE1}} = e^{-\beta(\mu_L - \epsilon_0)},$$
$$\frac{R_{CR0\,CE0}}{R_{CE0\,CR0}} = \frac{R_{CR1\,CE1}}{R_{CE1\,CR1}} = e^{-\beta(\epsilon_0 - \mu_R)} \tag{4}$$

[compare Eq. (4) with Eq. (2)]. Equations (3) and (4) ensure the thermodynamic consistency of the model, but do not yet completely specify the dynamics of y. We assume that the timescale of the stochastic dynamics of y due to thermal jumps is on the order of unity and our choice of the transition rates consistent with Eqs. (3) and (4) is shown in Table I. Please refer to Appendix A for a detailed discussion on the choice of the transition rates and corresponding timescales.

During every interaction interval of duration τ, the joint dynamics of the DQD and bit are described by a Markov jump process for the state variable $y = (x, b)$ in $\mathcal{G}_f$, with

TABLE I. Transition rates for jumps of the variable y in $\mathcal{G}_f$. $R_{y_i y_j}$ denotes the transition rate from y_j to y_i. Here we have taken $r = e^{-\beta\epsilon}$ with $\epsilon = (\epsilon_u - \epsilon_0) = (\epsilon_0 - \epsilon_l)$. These rates are used to construct the matrix $\mathbf{R}$, which is shown in Eq. (B1) in Appendix B.

$R_{CL0\,CR0}$	$= r$
$R_{CR0\,CL0}$	$= 1$
$R_{CL1\,CR1}$	$= r$
$R_{CR1\,CL1}$	$= 1$
$R_{BL0\,CL0}$	$= 1$
$R_{CL0\,BL0}$	$= r^2$
$R_{BL1\,CL1}$	$= 1$
$R_{CL1\,BL1}$	$= r^2$
$R_{BL0\,BR0}$	$= 1$
$R_{BR0\,BL0}$	$= 1$
$R_{BL1\,BR1}$	$= 1$
$R_{BR1\,BL1}$	$= 1$
$R_{AR0\,BR0}$	$= r^2$
$R_{BR0\,AR0}$	$= 1$
$R_{AR1\,BR1}$	$= r^2$
$R_{BR1\,AR1}$	$= 1$
$R_{AL0\,AR0}$	$= 1$
$R_{AR0\,AL0}$	$= r$
$R_{AL1\,AR1}$	$= 1$
$R_{AR1\,AL1}$	$= r$
$R_{AE0\,AL0}$	$= e^{-\beta(\mu_L - \epsilon_0)}$
$R_{AL0\,AE0}$	$= 1$
$R_{AE1\,AL1}$	$= e^{-\beta(\mu_L - \epsilon_0)}$
$R_{AL1\,AE1}$	$= 1$
$R_{CR0\,CE0}$	$= 1$
$R_{CE0\,CR0}$	$= e^{-\beta(\mu_R - \epsilon_0)}$
$R_{CR1\,CE1}$	$= 1$
$R_{CE1\,CR1}$	$= e^{-\beta(\mu_R - \epsilon_0)}$
$R_{BE0\,AE1}$	$= 1$
$R_{AE1\,BE0}$	$= 1$
$R_{CE0\,BE1}$	$= 1$
$R_{BE1\,CE0}$	$= 1$
$R_{AL0\,BL1}$	$= r$
$R_{BL1\,AL0}$	$= 1$
$R_{BR0\,CR1}$	$= 1$
$R_{CR1\,BR0}$	$= r$

transition rates shown in Table I. In a continuous time Markov jump process, the jump times follow a Poisson distribution as discussed in detail in Appendix C. At the end of each interaction interval, when a new bit b_{in} arrives, the state of the DQD x remains unchanged and the state of the interacting bit b takes on the value of the incoming bit b_{in}. Thus when the outgoing and incoming bit states differ, there is an effective *virtual jump*, due to the fact that the "old" interacting bit is replaced by the next bit in the memory tape.

D. Summary of the modeling strategy

Here we summarize our approach for creating an autonomous, memory-tape model of Maxwell's demon from the nonautonomous, feedback-controlled AA model. We first create a network representation of the states of the feedback-controlled model by identifying the dynamical states of the system ($\sigma \in \mathbf{\Sigma}$) and the states of the control parameter ($\lambda \in \mathbf{\Lambda}$). We then convert the control parameter λ to a stochastic dynamic variable that jumps among the states of $\mathbf{\Lambda}$. The joint state of the system and parameter is given by $x \equiv (\lambda, \sigma) \in \mathbf{V_x}$. The next step is to identify a network $\mathcal{G}_r = (\mathbf{V_x}, \mathbf{E_x})$ whose edges correspond to possible transitions. For thermodynamic consistency, the transition rates must satisfy Eqs. (1) and (2). There is no unique way to construct the network $\mathcal{G}_r$ and different choices of the allowed transitions lead to different memory-tape models. For our DQD system, we focused on designing a model that mimics the feedback-controlled model's behavior and is simple enough for analytical and semianalytical treatment.

Next, the DQD is connected to a sliding memory tape (information reservoir). By interacting with only the nearest bit on the tape, the DQD interacts with each bit for a fixed time τ. During that time, the coupling between the DQD and the interacting bit b occurs along those edges in the network $\mathcal{G}_r$ that correspond to the instantaneous feedback steps of the AA model. The bit coupling rules are chosen so that incoming bits in the 0 state bias the resulting current in one direction (CW in our model) and incoming bits in the 1 state bias it in the other direction. In this way a memory tape with a surplus of 0's or 1's generates an effective force, which can be harnessed to oppose the thermodynamic forces arising from (for example) reservoirs at different chemical potentials.

The joint state of the DQD and interacting bit is described by a variable $y \equiv (x, b)$ that evolves by a Markov jump process in the network $\mathcal{G}_f = (\mathbf{V_y}, \mathbf{E_y})$. As we assume the bit states 0 and 1 to be energetically degenerate, the transition rates in $\mathcal{G}_f$ follow from those in $\mathcal{G}_r$; see Eqs. (3) and (4).

While we illustrate our strategy with the AA model and a specific network structure of its dynamics, this approach can be implemented with other feedback controlled models where an underlying network structure can be identified and then modified in the similar fashion as our approach to obtain a memory-tape model.

IV. ANALYSIS AND RESULTS

A. Methods

Following Ref. [25], let $\mathbf{p}(t_n)$ be a column vector with nine entries that describes the probability distribution of the states of the DQD state variable x in $\mathcal{G}_r$ (in the order AE, BE, CE, BL, BR, AL, CR, AR, CL) at time $t_n \equiv n\tau$ that marks the start of an interaction interval. Each incoming bit is independently sampled from the same probability distribution, with p_0 (or p_1) denoting the probability of the bit to arrive in state 0 (or 1). It is convenient to specify this distribution by the single parameter $\delta = p_0 - p_1$, which measures the excess of 0's among the incoming bits. The statistical state of the variable $y \equiv (x, b)$ in $\mathcal{G}_f$ at time t_n (just after the arrival of the nth bit) is given by the 18-dimensional vector

$$\mathbf{p_f}(t_n) = \mathbf{M}\mathbf{p}(t_n), \quad \mathbf{M} = \begin{pmatrix} p_0\mathbf{I} \\ p_1\mathbf{I} \end{pmatrix}, \tag{5}$$

with $\mathbf{I}$ being a 9×9 identity matrix. The first nine elements of $\mathbf{p_f}(t)$ correspond to the bit state $b = 0$ and the last nine elements to the state $b = 1$. From $t = t_n$ to t_{n+1} the probability distribution in $\mathcal{G}_f$ evolves under the master equation

$$\frac{d}{dt}\mathbf{p_f}(t) = \mathbf{R}\mathbf{p_f}(t), \tag{6}$$

where $\mathbf{R}$ is the 18×18 rate matrix whose off-diagonal elements are the transition rates listed in Table I and whose diagonal elements are $R_{y_i y_i} = -\sum_{y_j \neq y_i} R_{y_j y_i}$; see Eq. (B1) for an explicit expression for $\mathbf{R}$. At the end of the interaction interval, just before the next bit arrives, the joint probability distribution is obtained from the solution of Eq. (6), namely

$$\mathbf{p_f}(t_n + \tau) = e^{\mathbf{R}\tau}\mathbf{M}\mathbf{p}(t_n). \tag{7}$$

To obtain the probability distribution of x in $\mathcal{G}_r$ at the end of the interaction interval, we project from the 18-state network $\mathcal{G}_f$ to the nine-state network $\mathcal{G}_r$,

$$\mathbf{p}(t_n + \tau) = \mathbf{P_D}e^{\mathbf{R}\tau}\mathbf{M}\mathbf{p}(t_n), \quad \mathbf{P_D} = (\mathbf{I} \quad \mathbf{I}). \tag{8}$$

Equivalently,

$$\mathbf{p}[(n+1)\tau] = \mathbf{T}\mathbf{p}(n\tau), \quad \mathbf{T} = \mathbf{P_D}e^{\mathbf{R}\tau}\mathbf{M}. \tag{9}$$

This transition matrix $\mathbf{T}$ (which depends on the parameter τ) evolves the probability distribution of x in $\mathcal{G}_r$ over a single interaction interval. The evolution over n successive intervals is described by the transition matrix $\mathbf{T}^n$. From the Perron-Frobenius theorem [65] it follows that any distribution $\mathbf{p}$ in $\mathcal{G}_r$ evolves asymptotically to a unique periodic steady state

$$\mathbf{q}_{\rm pss} = \lim_{n\to\infty} \mathbf{T}^n\mathbf{p}. \tag{10}$$

The periodic steady state $\mathbf{q}_{\rm pss}$ is a function of the interaction interval τ and can be calculated by solving for the invariant vector of the matrix $\mathbf{T}$,

$$\mathbf{T}\,\mathbf{q}_{\rm pss} = \mathbf{q}_{\rm pss}. \tag{11}$$

Once the periodic steady state for the DQD has been reached, the joint state of the DQD and bit at the start of every interaction interval is given by $\mathbf{M}\mathbf{q}_{\rm pss}$ and the joint state at a

time $t_n + \Delta t$, with $0 \leqslant \Delta t < \tau$, is

$$\mathbf{p_f}(t_n + \Delta t) = e^{\mathbf{R}\Delta t}\mathbf{M}\mathbf{q}_{\rm pss}. \tag{12}$$

For the remainder of this paper, when analyzing the behavior of our model, we will assume that the periodic steady state has been reached.

B. Thermodynamics of the memory-tape model

1. Calculation of work

Let the *circulation* $\Phi(\tau)$ denote the average number of electrons transferred from the left to the right reservoir during each interaction interval. The average chemical work performed by the DQD system per time interval τ is then

$$W(\tau) = (\mu_R - \mu_L)\Phi(\tau). \tag{13}$$

If the sign of $\mu_R - \mu_L$ is the same as that of $\Phi(\tau)$, then electrons flow from the lower to higher chemical potential, that is, against the thermodynamic force.

From Fig. 3 we see that

$$\begin{aligned}\Phi(\tau) &= \int_0^\tau dt\, J^r_{CR\to CE} = \int_0^\tau dt\, J^r_{CE\to BE} \\ &= \int_0^\tau dt\, J^r_{BE\to AE} = \int_0^\tau dt\, J^r_{AE\to AL},\end{aligned} \tag{14}$$

where $J^r_{x_j\to x_i} \equiv J^r_{x_i x_j}$ is the probability current along $x_j \to x_i$ in $\mathcal{G}_r$, projected from the corresponding currents in $\mathcal{G}_f$. We can determine $\Phi(\tau)$ by calculating any one of these integrals.

The probability current along $y_j \to y_i$ of $\mathcal{G}_f$ is

$$J_{y_i y_j} = R_{y_i y_j} p_{y_j}(t) - R_{y_j y_i} p_{y_i}(t). \tag{15}$$

When two edges $x_j 0 \leftrightarrow x_i 0$ and $x_j 1 \leftrightarrow x_i 1$ in $\mathcal{G}_f$ correspond to the edge $x_j \leftrightarrow x_i$ in $\mathcal{G}_r$, we have

$$J^r_{x_i x_j}(t) = J_{x_i 0\, x_j 0}(t) + J_{x_i 1\, x_j 1}(t), \tag{16}$$

but when the transition $x_j \to x_i$ is coupled with a bit flip $b' \to b''$, we have

$$J^r_{x_i x_j}(t) = J_{x_i b''\, x_j b'}(t). \tag{17}$$

Since the $CE \leftrightarrow BE$ transition is coupled to the bit flit $0 \leftrightarrow 1$, the edge $CE \leftrightarrow BE$ in $\mathcal{G}_r$ corresponds to a single edge, $CE0 \leftrightarrow BE1$ in $\mathcal{G}_f$; hence

$$\Phi(\tau) = \int_0^\tau dt\, J^r_{BE\ CE} = \int_0^\tau dt\, J_{BE1\ CE0}. \tag{18}$$

Moreover, since $BE1$ is connected to only one edge, $CE0 \leftrightarrow BE1$, we have $\dot{p}_{BE1} = J_{BE1\ CE0}$; see Fig. 4. Therefore,

$$\begin{aligned}\Phi(\tau) &= \int_0^\tau dt\, \dot{p}_{BE1} = [p_{BE1}(\tau) - p_{BE1}(0)] \\ &= [(e^{\mathbf{R}\tau} - \mathbf{I})\mathbf{M}\mathbf{q}_{\rm pss}]_{y=BE1},\end{aligned} \tag{19}$$

where we have used Eq. (12) to get to the second line. We will use this result in Sec. IV C 1.

2. Calculation of entropy change of the bit

Let p'_0 and p'_1 denote the probabilities of the outgoing bit to be in the states 0 and 1. These values are determined by summing over the appropriate states $y = (x, b)$ in $\mathcal{G}_f$ at the end of an interaction interval:

$$\begin{aligned}p'_0 &= \sum_{x\in V(\mathcal{G}_r)} (e^{\mathbf{R}\tau}\mathbf{M}\,\mathbf{q}_{\rm pss})_{y=(x,0)}, \\ p'_1 &= \sum_{x\in V(\mathcal{G}_r)} (e^{\mathbf{R}\tau}\mathbf{M}\,\mathbf{q}_{\rm pss})_{y=(x,1)}.\end{aligned} \tag{20}$$

The parameter

$$\delta' = p'_0 - p'_1 \tag{21}$$

specifies the distribution of the outgoing bit. The entropy corresponding to this distribution is $S' = -\sum_{i=0,1} p'_i \ln p'_i$, while that of the incoming bit is $S = -\sum_{i=0,1} p_i \ln p_i$. Thus, in the periodic steady state, the change in *single-symbol entropy* [41] of the interacting bit is $\Delta S = S' - S$. Because ΔS does not account for correlations that develop between successive outgoing bits, it provides only an upper bound on the net entropy change (per bit) of the information reservoir. We discuss this point in detail in the next section (IV B 3), in the context of the second law of thermodynamics.

3. First and the second law of thermodynamics

In the periodic steady state, the change in the internal energy of the DQD over one interaction interval is zero, on average. If chemical work is performed by the flow of electrons from low to high chemical potential, then the energy required for this process must be extracted as heat from the thermal reservoir that maintains the entire system at a fixed temperature T. We write the first law of thermodynamics at the periodic steady state for this model as

$$Q(\tau) = W(\tau) = (\mu_R - \mu_L)\Phi(\tau), \tag{22}$$

where $Q(\tau)$ is the average heat extracted from the thermal reservoir, per interaction interval.

In Refs. [41,42], a general form of the second law for the information ratchets, called the information processing second law (IPSL), was derived. In the periodic steady state the IPSL is written as

$$(\ln 2)\Delta h_\mu \geqslant \beta W, \tag{23}$$

where Δh_μ is the change in the Shannon entropy rate, see Refs. [41,42], and W is the average work extracted in one interaction interval. The entropy rate Δh_μ includes the effect of correlations among the bits in the incoming and outgoing bit streams. In our model we have assumed that incoming bits are uncorrelated with each other and have been generated through a *memoryless* [42] process. For finite τ, the outgoing bits become correlated with each other and thus the output is *memoryful* [42]. However, in the limit $\tau \to \infty$ these correlations become lost and the Shannon entropy rate Δh_μ reduces to the change in single-symbol entropy $\Delta S/(\ln 2)$; hence for our model Eq. (23) becomes (in that limit)

$$\Delta S \geqslant \beta W. \tag{24}$$

Equation (23) is a general result for any memory-tape Maxwell demon and Eq. (24) is a limiting case of the IPSL when correlations are neglected. When correlations are non-negligible, Eq. (23) can identify functional modes of operation that are not indicated by Eq. (24); see Refs. [41,44,46].

However, it is common to use the single symbol entropy for the analysis of memory-tape models [25,26,29,30,36] and Eq. (24) has been previously derived in the context of Hamiltonian dynamics [24] and stochastic dynamics [31]. In our model, we ignore the effect of the correlations among the bits for simplicity and assume the validity of Eq. (24) as an approximation to Eq. (23) even for finite τ. The analysis of the effect of correlations among the bits and calculation of Δh_μ is outside the scope of this article; see Ref. [46] for the Δh_μ calculation in context of the MJ model. Henceforth, by "entropy" we always refer to single-symbol entropy unless otherwise specified.

C. Analytical results for $\tau \to \infty$

1. Thermodynamic quantities

There are two relevant timescales in our model. We have taken the timescale associated with the thermal jumps in $\mathcal{G}_f$, which are governed by Eq. (6), to be of order unity. The other timescale is the parameter τ that defines how long the DQD interacts with each bit. From the Perron-Frobenius theorem [65], we have

$$\lim_{\tau\to\infty} e^{\mathbf{R}\tau}\mathbf{p_f} = \mathbf{\Pi}, \quad \forall\, \mathbf{p_f}, \tag{25}$$

where $\mathbf{R\Pi} = \mathbf{0}$. The expression for $\mathbf{\Pi}$ is given in Eq. (B2) in Appendix B. If τ is sufficiently large, then Eq. (11) becomes

$$\mathbf{q}^{\infty}_{\rm pss} = \lim_{\tau\to\infty} \mathbf{P_D} e^{\mathbf{R}\tau}\mathbf{M}\mathbf{q}_{\rm pss} = \mathbf{P_D}\mathbf{\Pi}. \tag{26}$$

Using Eqs. (B2) and (26), we get

$$\mathbf{q}^{\infty}_{\rm pss} = \mathcal{N}\left[\frac{2\kappa_L}{r}\ \frac{(\kappa_L+\kappa_R)}{r}\ \frac{2\kappa_R}{r}\ \frac{2}{r^2}\ \frac{2}{r^2}\ \frac{2}{r}\ \frac{2}{r}\ 2\ 2\right]^T,$$
$$\mathcal{N} = \frac{r^2}{4(1+r+r^2)+3r(\kappa_L+\kappa_R)}, \tag{27}$$

where $\kappa_L = e^{-\beta(\mu_L-\epsilon_0)}$, $\kappa_R = e^{-\beta(\mu_R-\epsilon_0)}$, and $r = e^{-\beta\epsilon}$, with $\epsilon = (\epsilon_u - \epsilon_0) = (\epsilon_0 - \epsilon_l)$. Note that here we have taken symmetric energy gaps in the dots for simplicity of calculation and conciseness of results. The method of analysis would be the same if ϵ_u and ϵ_l were taken as free parameters.

In the $\tau \to \infty$ limit, the circulation (Φ_∞) can be calculated using Eq. (19). The probabilities $p_{BE1}(0)$ and $p_{BE1}(\infty)$ are given by the $BE1$ elements of $\mathbf{M}\mathbf{q}^{\infty}_{\rm pss}$ and $\mathbf{\Pi}$, respectively. Using Eqs. (13), (19), (25), and (27) we get

$$W_\infty = \frac{\mathcal{N}(\mu_R-\mu_L)}{r}\left[\left(\frac{1+\delta}{2}\right)\kappa_R - \left(\frac{1-\delta}{2}\right)\kappa_L\right]. \tag{28}$$

Using Eqs. (25), (20), and (21), we can describe the distribution of the outgoing bits as $p'_{0,1} = (1 \pm \delta')/2$, where

$$\delta' = \frac{r(\kappa_L-\kappa_R)}{4(1+r+r^2)+3r(\kappa_L+\kappa_R)}, \tag{29}$$

which can be used to calculate the entropy of the outgoing bits as $S' = -\sum_{i=0,1} p'_i \ln p'_i \in [0, \ln 2]$.

2. Operational mode phase diagram

In the limit $\tau \to \infty$, bits in the outgoing bit stream are uncorrelated and thus Eqs. (23) and (24) are equivalent and both the final distribution δ' and the entropy of the outgoing bit become independent of δ; see Eq. (29). The entropy change $\Delta S_\infty \equiv \lim_{\tau\to\infty}(S' - S)$ is a symmetric concave upwards function of δ with a negative value at its minimum ($\min_\delta\{\Delta S_\infty\} < 0$) at $\delta = 0$ when $\mu_L \neq \mu_R$. Thus, in the region with $|\delta| < |\delta'|$ [shaded red in Fig. 5(a)], we have $\Delta S_\infty < 0$ and $W_\infty < 0$ [using Eq. (24)]. By Eq. (29), we see that when

$$|\delta| < |\delta'| = \left|\frac{r(\kappa_L-\kappa_R)}{4(1+r+r^2)+3r(\kappa_L+\kappa_R)}\right|, \tag{30}$$

information is erased from the incoming memory tape and the system consumes work, i.e., it acts as a Landauer eraser. Therefore, for a given value of $\Delta\mu = \mu_R - \mu_L$, the Landauer eraser region in the operational mode phase diagram is bounded by $\pm\delta'$, as indicated by the red regions in Fig. 6.

By Eq. (24), $W_\infty > 0$ implies $\Delta S_\infty > 0$. Let δ^* denote the value of δ at which $\Phi_\infty = W_\infty/\Delta\mu$ changes its sign, for fixed μ_R and μ_L. Using Eq. (28) we obtain

$$\delta^* = \frac{\kappa_L - \kappa_R}{\kappa_L + \kappa_R}. \tag{31}$$

Thus $W_\infty > 0$ when $\delta > \delta^*$ and $\mu_R > \mu_L$ or when $\delta < \delta^*$ and $\mu_R < \mu_L$. In these regions of parameter space, shown in green in Fig. 6, the system produces work at the cost of writing information to the memory tape and the DQD acts as an information engine.

In the regions of parameter space where $\Delta S_\infty > 0 > W_\infty$, information is written to the memory tape and the system consumes work; hence the model is a *dud* [25].

D. Semianalytical results for finite τ

For finite interaction time τ, we can numerically diagonalize the transition rate matrix as $\mathbf{R} = \mathbf{U}\mathbf{D_R}\mathbf{V}$, where $\mathbf{D_R}$ is diagonal and $\mathbf{UV} = \mathbf{VU} = I$. We then have

$$\mathbf{T} = \mathbf{P_D}\mathbf{U}e^{\mathbf{D_R}\tau}\mathbf{V}\mathbf{M} \tag{32}$$

and the evaluation of $e^{\mathbf{D_R}\tau}$ is straightforward. Once $\mathbf{T}$ is obtained in this manner, the periodic steady state $\mathbf{q_{pss}}$ is calculated using Eq. (11) and thermodynamic quantities are determined as described in Sec. IV B. Following this semianalytical approach, we have obtained phase diagrams for different values of τ, using the second law inequality Eq. (24), which is now the single symbol approximation to the IPSL in Eq. (23). Figure 7 shows these phase diagrams. The competition between the effects of bit coupling (δ) and the thermodynamic bias ($\Delta\mu$) determines the direction of probability current, i.e., the sign of Φ, in the network. With increasing values of τ, the system has more time to relax to the equilibrium state $\mathbf{\Pi}$ before a new bit arrives and the phase diagram approaches the one shown in Fig. 6.

In our model, the information engine region ($W > 0$) appears only in the first and third quadrants of the phase diagrams. In these regions an increase in $|\Delta\mu|$ increases the effective thermodynamic forces and suppresses the information engine region for a fixed value of δ, as seen in Figs. 6 and 7.

For small values of τ, the frequency of the virtual jumps in $\mathcal{G}_f$ (see Sec. III C 2) increases, as bits get replaced more frequently. These virtual jumps drive the probability current

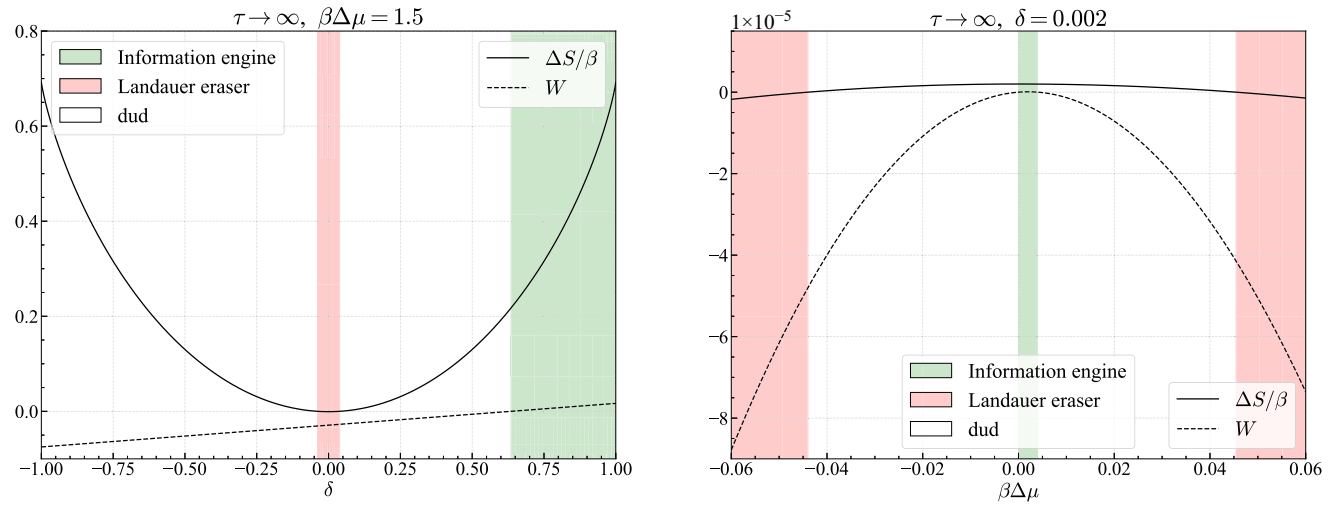

FIG. 5. Plots of $\Delta S/\beta$ and W when (a) δ is varied at fixed $\mu_R = 1.5$ and $\mu_L = 0$ and (b) $\beta\Delta\mu$ is varied by changing μ_R at fixed $\mu_L = 0$ and $\delta = 0.002$. In both cases we set $\beta = 1$, $r = e^{-1}$, $\epsilon_0 = 0$, and we take the limit $\tau \to \infty$. In both plots we see that $\Delta S \geqslant \beta W$ is satisfied. The regions corresponding to the information engine ($\Delta S > 0, W > 0$), Landauer eraser ($\Delta S < 0, W < 0$), and dud ($\Delta S > 0, W < 0$) are shaded green, red, and white, respectively. (a) δ variation. (b) $\Delta\mu$ variation.

against the thermodynamic force in $\mathcal{G}_r$. Hence when τ is increased the information engine region decreases; see Fig. 7.

The entropy $S(\delta) = -\sum_i p_i \ln p_i$, with $p_{0,1}(\delta) = (1 \pm \delta)/2$, is a concave downward function with a maximum at $\delta = 0$. As a result, when $\delta = 0$ and $\delta' \neq 0$ we have $\Delta S = S(\delta') - S(\delta) < 0$. This explains why the Landauer eraser region ($\Delta S < 0$) contains the entire $\delta = 0$ axis in the phase diagram (except for the origin $\delta = \beta\Delta\mu = 0$, where $\Delta S = 0$).

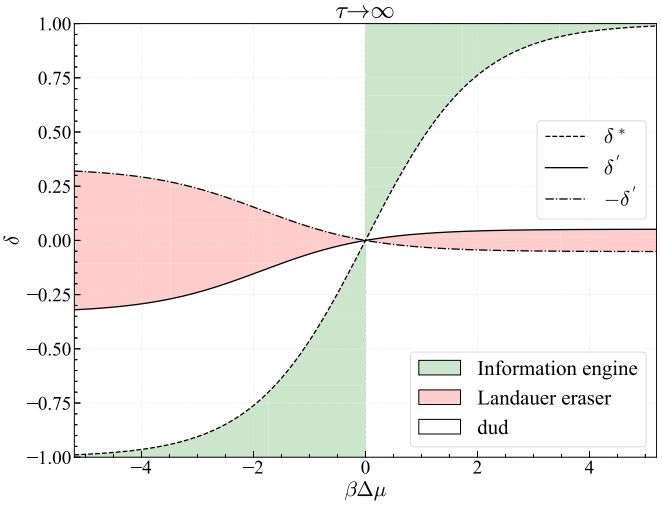

FIG. 6. Analytically obtained phase diagram when $\tau \to \infty$. In the green region the system operates as an information engine ($\Delta S > 0, W > 0$) and in the red region it acts as a Landauer eraser. The critical parameter values δ^*, δ', and $-\delta'$ are shown as functions of $\beta\Delta\mu$ with $\Delta\mu = \mu_R - \mu_L$ and with $\mu_L = 0$. We have taken $\epsilon_0 = 0$, $\beta = 1$, and $r = e^{-1}$ here.

E. Stochastic simulation

We have also performed stochastic simulations of the system. The variable $y = (\lambda, \sigma, b)$ was initialized by sampling $x = (\lambda, \sigma)$ from the distribution $\mathbf{q}_{\mathbf{pss}}$ and b from the distribution δ. During each bit interaction interval, y evolves under a Markov jump process, with the rates listed in Table I. At the end of each interval, the value of b is replaced by the (randomly sampled) state of the incoming bit. See Appendix C for further simulation details.

Figures 8(a) and 8(b) show work and entropy production when the system acts as a Landauer eraser and as an information engine, respectively. The total change in entropy ($\sum_n \Delta S_n$) of the memory tape was calculated by summing the change in single symbol entropy over each bit (ΔS_n) in the memory tape. Similarly, total work ($\sum_n W_n$) was obtained by summing over the work done over each interval (W_n). In these figures, the semianalytical results obtained by the approach described in Sec. IV D are represented by straight lines with slopes $\Delta S/\tau$ and W/τ. $N = 10^5$ trajectories were generated and statistical errors in ΔS_n and W_n were calculated using the bootstrap method, by resampling $B = 10^5$ times with replacements [66]. The increasing errors in $\sum_n \Delta S_n$ and $\sum_n W_n$ reflect the accumulation of statistical errors with each additional interaction interval.

V. CONCLUSION

We have presented a strategy for constructing a memory-tape model of Maxwell's demon, from a feedback-controlled model. We have illustrated this strategy using the Annby-Andersson model [56], a feedback-controlled Maxwell's demon in a double quantum dot (DQD). In our approach, we replace the feedback controller with a stochastic variable evolving under the same thermal environment as the DQD.

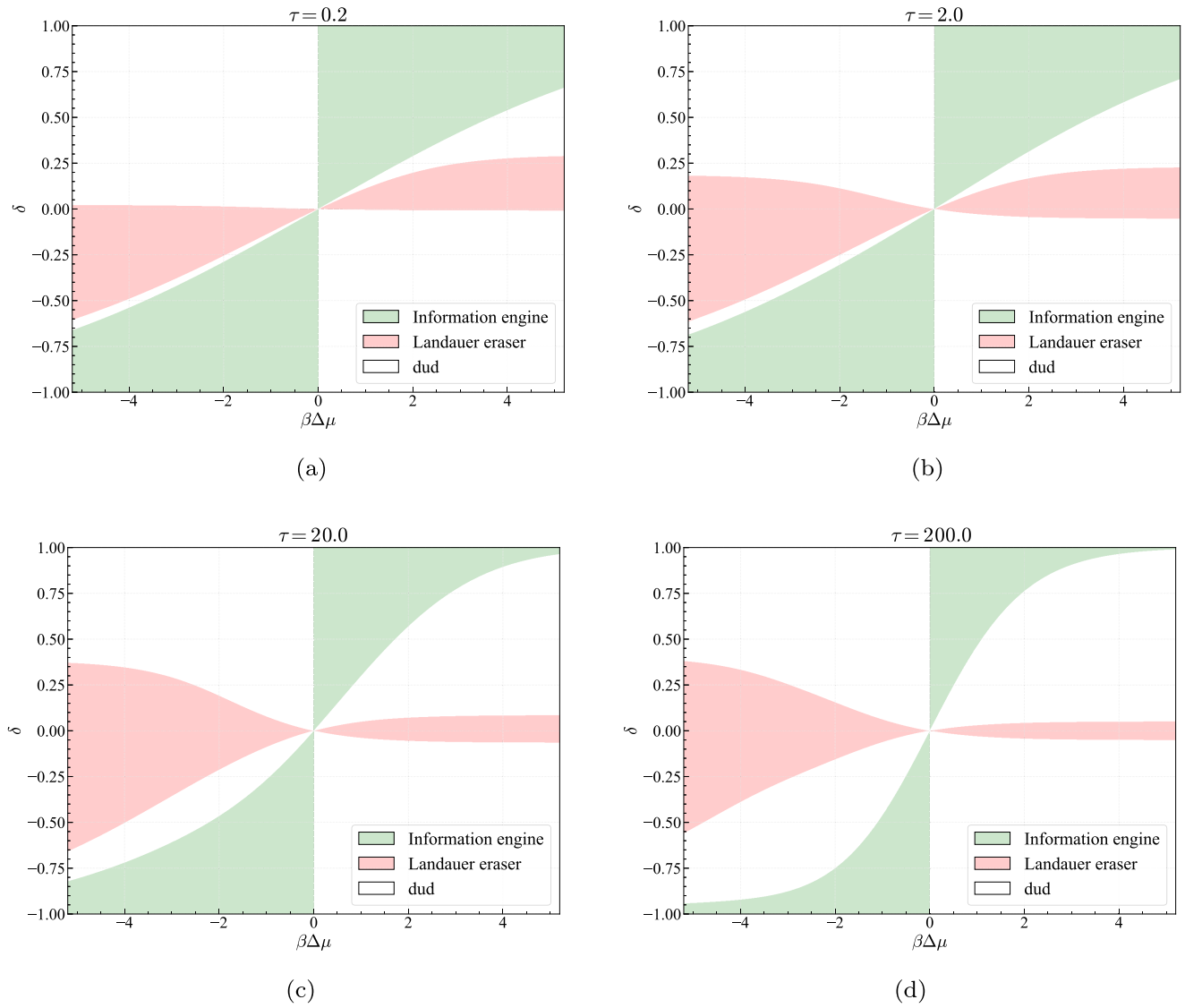

FIG. 7. Numerically obtained phase diagrams for different values of the interaction time, $\tau = 0.2$, 2, 20, and 200. For finite τ, the final distribution of the memory-tape (δ') depends on the initial distribution (δ), but this dependence vanishes in the limit $\tau \to \infty$. With increasing τ, the phase diagram approaches the one shown in Fig. 6. We have fixed $r = e^{-1}$, $\beta = 1$, and $\epsilon_0 = 0$. (a) Phase diagram ($\tau = 0.2$). (b) Phase diagram ($\tau = 2.0$). (c) Phase diagram ($\tau = 20.0$). (d) Phase diagram ($\tau = 200.0$).

We then couple our system to an information reservoir and design suitable bit interaction rules to mimic the effects of the feedback controller. In analyzing our model, we obtained an exact solution in the limit of infinitely long interaction time τ and used a semianalytical approach involving numerical matrix diagonalization for finite τ. As illustrated by these results as well as stochastic simulations, our model can act both as an information engine and as a Landauer eraser, for suitable parameter values.

Our research strengthens the connection between two paradigms of information thermodynamics: Maxwell's original, nonautonomous paradigm of a "nimble-fingered" demon performing feedback control at the level of thermal fluctuations and the autonomous paradigm, due to Bennett [20], in which the demon is replaced by a physical gadget, thermodynamically driven by the continual randomization of a stream of bits (the memory tape). In effect, given a demon, we show how to design a gadget that mimics it.

Our approach makes use of the underlying network structure of a feedback-controlled system and it relates to recent stochastic thermodynamic studies of bipartite systems [57,67,68]. Specifically, the dynamics of $y = (\lambda, \sigma, b)$ in $\mathcal{G}_f$ can be described as bipartite system dynamics by splitting y in two random variables σ and $\bar{x} \equiv (\lambda, b)$ that do not change simultaneously. This is in contrast with the original MJ model [25], which lacks the bipartite structure; see [57].

Double quantum dot systems are promising candidates for the experimental implementation of information engines [69]. We note that while there have been a number of realizations of feedback-controlled demons [1,2], experimental realizations

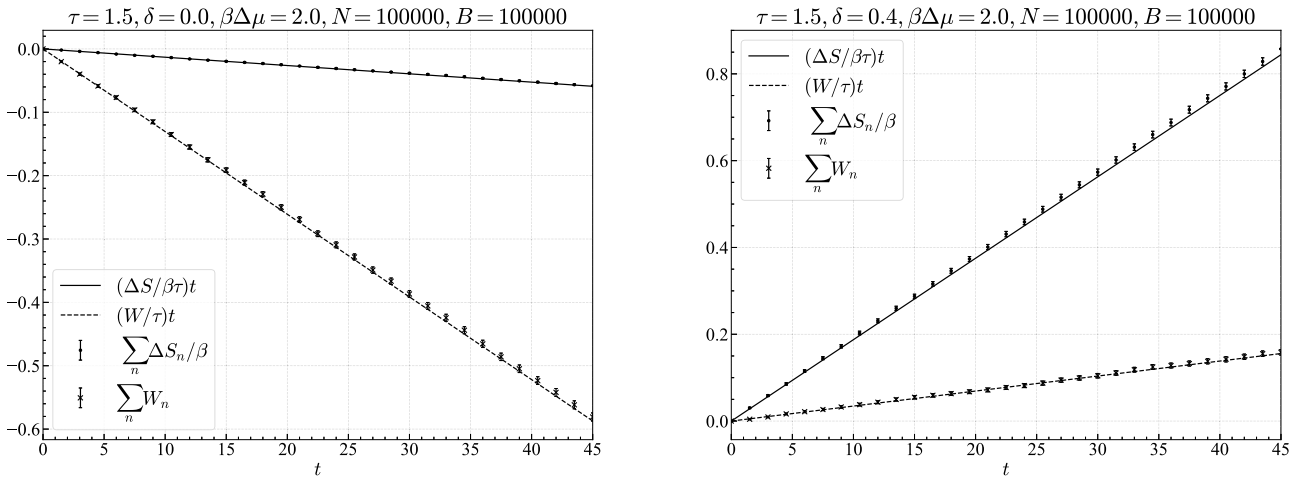

FIG. 8. Work and entropy production in (a) the Landauer eraser mode and (b) the information engine mode. Semianalytical results and stochastic simulation results are compared. ΔS_n and W_n represent the change in single symbol entropy of the nth bit and average extracted work in the nth interval. For all the simulations, we have taken $\beta = 1$, $r = e^{-1}$, and $\epsilon_0 = 0$. Errors are calculated with the bootstrap method.

of memory-tape models are yet to be explored. By showing how to design a memory-tape model that mimics a feedback controlled system, our approach may be useful in the design of physical implementations of autonomous information engines.

Although our analysis has been entirely at the level of classical stochastic dynamics, it would be worth studying analogous quantum models (see, e.g., Ref. [38]). A future research direction might explore design principles for quantum analogs of the memory-tape model. Lastly, we limited our discussion of the information-theoretic aspects of this model to the single symbol entropy. The study of the effects of correlations among the bits offers another avenue for future research.

ACKNOWLEDGMENTS

This research was supported by FQXi Grant No. FQXi-IAF19-07 from the Foundational Questions Institute Fund, a donor advised fund of the Silicon Valley Community Foundation. We thank G. De Sousa, B. Annby-Andersson, F. Bakhshinezhad, P. Samuelsson, and P. P. Potts for fruitful discussions and valuable feedback on the manuscript.

APPENDIX A: TRANSITION RATES AND THE DETAILED BALANCE RELATIONS

Equations (3) and (4) together give ratios of the transition rates which guarantee the thermodynamic consistency of the model but do not completely define the transition rates for the dynamics of y in the network $\mathcal{G}_f$. Thus there is a freedom in the choice of transition rates along the edges of $\mathcal{G}_f$ as long as the rations in Eqs. (3) and (4) are maintained. When there is no coupling with an electron reservoir, we have taken

$$R_{y_i y_j} = \Gamma\, e^{-\beta(E_i - E_j)}, \;\; R_{y_j y_i} = \Gamma, \tag{A1}$$

for $E_i > E_j$, which satisfies Eq. (3). The prefactor Γ is the inverse timescale of the thermal jumps of the system and we have taken $\Gamma = 1$. For example, the transition rates along the $CL0 - CR0$ edge are given as $R_{CL0\,CR0} = e^{-\beta(\epsilon_u - \epsilon_0)} = e^{-\beta\epsilon} = r$ and $R_{CR0\,CL0} = 1$, where we have taken $(\epsilon_u - \epsilon_0) = (\epsilon_0 - \epsilon_l) = \epsilon$ and $r = e^{-\beta\epsilon}$. We have assigned the rest of the rates in Table I in a similar fashion when there is no coupling with an electron reservoir.

When there is an exchange of electron with the dot and the electron reservoir ($\sigma = L/R \leftrightarrow \sigma = E$), Eq. (4) ensures the thermodynamic consistency of the transition rates. Here we use the convention that when the electron enters the dot from the electron reservoir ($\sigma = E \rightarrow \sigma = L/R$) the transition rate is Γ_{res} and when the electron leaves the dot to the electron reservoir ($\sigma = L/R \rightarrow \sigma = E$) the transition rates are given as $\Gamma_{\text{res}} e^{-\beta(\mu_{L/R} - \epsilon_0)}$, which is consistent with Eq. (4). For simplicity we have also taken $\Gamma_{\text{res}} = 1$. Thus, for example, $R_{AE0\,AL0} = e^{-\beta(\mu_L - \epsilon_0)}$ and $R_{AL0\,AE0} = 1$. The other transitions involving the electron reservoirs are similarly set, as seen in Table I.

Note that the shortest timescale of the dynamics of the thermal jumps is given as $1/\max\{\Gamma, \Gamma_{\text{res}}\}$, which we have taken as 1 in our model. It should be noted that the timescale of the thermal jump is in general different from the duration of the bit interaction interval τ, which is another temporal parameter of our model.

APPENDIX B: RATE MATRIX AND UNIQUE STATIONARY STATE FOR $\mathcal{G}_f$

The rate matrix $\mathbf{R}$ and stationary distribution $\mathbf{\Pi}$ are

$$\mathbf{R} = \begin{pmatrix}
\boldsymbol{-1} & 0 & 0 & 0 & 0 & \boldsymbol{\kappa_L} & 0 & 0 & 0 & 0 & 0 & 0 & 0 & 0 & 0 & 0 & 0 & 0 \\
0 & \boldsymbol{-1} & 0 & 0 & 0 & 0 & 0 & 0 & 0 & \boldsymbol{1} & 0 & 0 & 0 & 0 & 0 & 0 & 0 & 0 \\
0 & 0 & \boldsymbol{-2} & 0 & 0 & 0 & \boldsymbol{\kappa_R} & 0 & 0 & 0 & \boldsymbol{1} & 0 & 0 & 0 & 0 & 0 & 0 & 0 \\
0 & 0 & 0 & \boldsymbol{K_1} & \boldsymbol{1} & 0 & 0 & 0 & \boldsymbol{1} & 0 & 0 & 0 & 0 & 0 & 0 & 0 & 0 & 0 \\
0 & 0 & 0 & \boldsymbol{1} & \boldsymbol{K_2} & 0 & 0 & \boldsymbol{1} & 0 & 0 & 0 & 0 & 0 & 0 & 0 & \boldsymbol{1} & 0 & 0 \\
\boldsymbol{1} & 0 & 0 & 0 & 0 & \boldsymbol{K_3} & 0 & \boldsymbol{1} & 0 & 0 & 0 & 0 & \boldsymbol{r} & 0 & 0 & 0 & 0 & 0 \\
0 & 0 & \boldsymbol{1} & 0 & 0 & 0 & \boldsymbol{K_4} & 0 & \boldsymbol{1} & 0 & 0 & 0 & 0 & 0 & 0 & 0 & 0 & 0 \\
0 & 0 & 0 & 0 & \boldsymbol{r^2} & \boldsymbol{r} & 0 & \boldsymbol{-2} & 0 & 0 & 0 & 0 & 0 & 0 & 0 & 0 & 0 & 0 \\
0 & 0 & 0 & \boldsymbol{r^2} & 0 & 0 & \boldsymbol{r} & 0 & \boldsymbol{-2} & 0 & 0 & 0 & 0 & 0 & 0 & 0 & 0 & 0 \\
0 & \boldsymbol{1} & 0 & 0 & 0 & 0 & 0 & 0 & 0 & \boldsymbol{-2} & 0 & 0 & 0 & 0 & \boldsymbol{\kappa_L} & 0 & 0 & 0 \\
0 & 0 & \boldsymbol{1} & 0 & 0 & 0 & 0 & 0 & 0 & 0 & \boldsymbol{-1} & 0 & 0 & 0 & 0 & 0 & 0 & 0 \\
0 & 0 & 0 & 0 & 0 & 0 & 0 & 0 & 0 & 0 & 0 & \boldsymbol{-1} & 0 & 0 & 0 & \boldsymbol{\kappa_R} & 0 & 0 \\
0 & 0 & 0 & 0 & 0 & \boldsymbol{1} & 0 & 0 & 0 & 0 & 0 & 0 & \boldsymbol{K_2} & \boldsymbol{1} & 0 & 0 & 0 & \boldsymbol{1} \\
0 & 0 & 0 & 0 & 0 & 0 & 0 & 0 & 0 & 0 & 0 & 0 & \boldsymbol{1} & \boldsymbol{K_1} & 0 & 0 & \boldsymbol{1} & 0 \\
0 & 0 & 0 & 0 & 0 & 0 & 0 & 0 & 0 & \boldsymbol{1} & 0 & 0 & 0 & 0 & \boldsymbol{K_5} & 0 & \boldsymbol{1} & 0 \\
0 & 0 & 0 & 0 & \boldsymbol{r} & 0 & 0 & 0 & 0 & 0 & 0 & \boldsymbol{1} & 0 & 0 & 0 & \boldsymbol{K_6} & 0 & \boldsymbol{1} \\
0 & 0 & 0 & 0 & 0 & 0 & 0 & 0 & 0 & 0 & 0 & 0 & 0 & \boldsymbol{r^2} & \boldsymbol{r} & 0 & \boldsymbol{-2} & 0 \\
0 & 0 & 0 & 0 & 0 & 0 & 0 & 0 & 0 & 0 & 0 & 0 & \boldsymbol{r^2} & 0 & 0 & \boldsymbol{r} & 0 & \boldsymbol{-2}
\end{pmatrix}, \tag{B1}$$

$$\mathbf{\Pi} = \frac{r^2}{4(1+r+r^2)+3r(\kappa_L+\kappa_R)} \begin{bmatrix}
\kappa_L r^{-1} \\ \kappa_L r^{-1} \\ \kappa_R r^{-1} \\ r^{-2} \\ r^{-2} \\ r^{-1} \\ r^{-1} \\ 1 \\ 1 \\ \kappa_L r^{-1} \\ \kappa_R r^{-1} \\ \kappa_R r^{-1} \\ r^{-2} \\ r^{-2} \\ r^{-1} \\ r^{-1} \\ 1 \\ 1
\end{bmatrix}, \tag{B2}$$

where $\kappa_L = e^{-\beta(\mu_L-\epsilon_0)}$, $\kappa_R = e^{-\beta(\mu_R-\epsilon_0)}$, $K_1 = -r^2-1$, $K_2 = -r^2-r-1$, $K_3 = -\kappa_L - r - 1$, $K_4 = -\kappa_R - r$, $K_5 = -\kappa_L - r$, and $K_6 = -\kappa_R - r - 1$. Here the states in $V(\mathcal{G}_f)$ are ordered as follows: ($AE0$, $BE0$, $CE0$, $BL0$, $BR0$, $AL0$, $CR0$, $AR0$, $CL0$, $AE1$, $BE1$, $CE1$, $BL1$, $BR1$, $AL1$, $CR1$, $AR1$, $CL1$).

APPENDIX C: DETAILS OF STOCHASTIC SIMULATION SCHEME

a. Poisson jumps

We implement the Gillespie Algorithm [70–72] to simulate the continuous time Markov jump process for y in $\mathcal{G}_f$, when the DQD system is interacting with a bit. If a system is in state y_j at time t, then the time interval for the next jump event is generated from the Poisson distribution as follows:

$$\Delta t = \frac{1}{\sum_{y\neq y_j} R_{yy_j}} \ln \frac{1}{\xi_1}, \tag{C1}$$

where ξ_1 is sampled uniformly in the interval (0,1]. After remaining in the state y_j over the time interval $[t, t+\Delta t)$, the system jumps to a new state (say $y_{j'}$). To find $y_{j'}$, all states in $V(\mathcal{G}_f)$ are arranged in order [say, $(0, 1, 2, \ldots, 16, 17)$]; then j' is chosen as the smallest integer label of the ordered states that satisfies

$$\frac{\sum_{i=0, y_i\neq y_j}^{j'} R_{y_i y_j}}{\sum_{y\neq y_j} R_{yy_j}} > \xi_2, \tag{C2}$$

where ξ_2 is sampled uniformly in the interval (0,1].

b. Virtual jumps

Virtual jumps occur when a new bit arrives. Specifically, if $y = (x_j, b_n)$ at time $t \in [n\tau, (n+1)\tau]$ and if $t + \Delta t > (n+1)\tau$, then, instead of generating a jump using Eq. (C2), a new bit state is generated at time $(n+1)\tau$.

The new incoming bit is sampled with probability p_0 (p_1) to be in state $b_{n+1} = 0$ ($b_{n+1} = 1$), the state y is updated

to $y_{j'} \equiv (x_j, b_{n+1})$, and the time is set to $t = (n+1)\tau$. We express this update rule as

$$b_{n+1} = \begin{cases} 0, & \text{with probability } p_0, \\ 1, & \text{with probability } p_1, \end{cases} \tag{C3}$$

$$y\,[(n+1)\tau] = (x_j, b_{n+1}), \tag{C4}$$

when $t + \Delta t > (n+1)\tau$. If $b_{n+1} \neq b_n$, then this update constitutes a virtual jump; otherwise, the state of y is unchanged.

[1] A. Rex, Maxwell's demon–a historical review, Entropy **19**, 240 (2017).

[2] J. M. R. Parrondo, J. M. Horowitz, and T. Sagawa, Thermodynamics of information, Nat. Phys. **11**, 131 (2015).

[3] M. Smoluchowski, Experimentell nachweisbare, der üblichen thermodynamik widersprechende molekularphänomene, Pisma Mariana Smoluchowskiego **2**, 226 (1927).

[4] M. Planck, P. Debye, W. Nernst, M. Smoluchowski, A. Sommerfeld, and H. Lorentz, *Vorträge über die kinetische theorie der materie und der elektrizität: gehalten in Göttingen auf einladung der Kommission der Wolfskehlstiftung*, Mathematische Vorlesungen an der Universität Göttingen (B.G. Teubner, Leipzig, 1914).

[5] P. A. Skordos and W. H. Zurek, Maxwell's demon, rectifiers, and the second law: Computer simulation of smoluchowski's trapdoor, Am. J. Phys. **60**, 876 (1992).

[6] L. Szilard, über die entropieverminderung in einem thermodynamischen system bei eingriffen intelligenter wesen, Z. Phys. **53**, 840 (1929).

[7] R. Feynman, R. Leighton, and M. Sands, *The Feynman Lectures on Physics, Vol. I: The New Millennium Edition: Mainly Mechanics, Radiation, and Heat*, The Feynman Lectures on Physics (Basic Books, New York, 2011).

[8] P. Reimann, Brownian motors: noisy transport far from equilibrium, Phys. Rep. **361**, 57 (2002).

[9] M. Esposito and G. Schaller, Stochastic thermodynamics for "Maxwell demon" feedbacks, Europhys. Lett. **99**, 30003 (2012).

[10] T. Sagawa and M. Ueda, Fluctuation Theorem with Information Exchange: Role of Correlations in Stochastic Thermodynamics, Phys. Rev. Lett. **109**, 180602 (2012).

[11] T. Sagawa and M. Ueda, Nonequilibrium thermodynamics of feedback control, Phys. Rev. E **85**, 021104 (2012).

[12] S. Lahiri, S. Rana, and A. Jayannavar, Fluctuation theorems in the presence of information gain and feedback, J. Phys. A: Math. Theor. **45**, 065002 (2012).

[13] J. M. Horowitz and S. Vaikuntanathan, Nonequilibrium detailed fluctuation theorem for repeated discrete feedback, Phys. Rev. E **82**, 061120 (2010).

[14] P. P. Potts and P. Samuelsson, Detailed Fluctuation Relation for Arbitrary Measurement and Feedback Schemes, Phys. Rev. Lett. **121**, 210603 (2018).

[15] Q. Zeng and J. Wang, New fluctuation theorems on Maxwell's demon, Sci. Adv. **7**, eabf1807 (2021).

[16] U. Seifert, Stochastic thermodynamics, fluctuation theorems and molecular machines, Rep. Prog. Phys. **75**, 126001 (2012).

[17] S. Ito and T. Sagawa, Information Thermodynamics on Causal Networks, Phys. Rev. Lett. **111**, 180603 (2013).

[18] N. Shiraishi, S. Ito, K. Kawaguchi, and T. Sagawa, Role of measurement-feedback separation in autonomous Maxwell's demons, New J. Phys. **17**, 045012 (2015).

[19] C. H. Bennett, Logical reversibility of computation, IBM J. Res. Dev. **17**, 525 (1973).

[20] C. Bennett, The thermodynamics of computation–a review, Int. J. Theor. Phys. **21**, 905 (1982).

[21] C. H. Bennett, Notes on landauer's principle, reversible computation, and Maxwell's demon, Stud. History Philos. Sci. Part B **34**, 501 (2003).

[22] R. Landauer, Irreversibility and heat generation in the computing process, IBM J. Res. Dev. **5**, 183 (1961).

[23] R. Landauer, Information is physical, Phys. Today **44**, 5, 23 (1991).

[24] S. Deffner and C. Jarzynski, Information Processing and the Second Law of Thermodynamics: An Inclusive, Hamiltonian Approach, Phys. Rev. X **3**, 041003 (2013).

[25] D. Mandal and C. Jarzynski, Work and information processing in a solvable model of Maxwell's demon, Proc. Natl. Acad. Sci. USA **109**, 11641 (2012).

[26] D. Mandal, H. T. Quan, and C. Jarzynski, Maxwell's Refrigerator: An Exactly Solvable Model, Phys. Rev. Lett. **111**, 030602 (2013).

[27] Z. Lu, D. Mandal, and C. Jarzynski, Engineering Maxwell's demon, Phys. Today **67**, 8, 60 (2014).

[28] Z. Lu and C. Jarzynski, A programmable mechanical Maxwell's demon, Entropy **21**, 65 (2019).

[29] A. C. Barato and U. Seifert, An autonomous and reversible Maxwell's demon, Europhys. Lett. **101**, 60001 (2013).

[30] A. C. Barato and U. Seifert, Unifying Three Perspectives on Information Processing in Stochastic Thermodynamics, Phys. Rev. Lett. **112**, 090601 (2014).

[31] A. C. Barato and U. Seifert, Stochastic thermodynamics with information reservoirs, Phys. Rev. E **90**, 042150 (2014).

[32] J. Hoppenau and A. Engel, On the energetics of information exchange, Europhys. Lett. **105**, 50002 (2014).

[33] R. E. Spinney, M. Prokopenko, and D. Chu, Information ratchets exploiting spatially structured information reservoirs, Phys. Rev. E **98**, 022124 (2018).

[34] P.-Y. Peng and C.-K. Duan, A Maxwell demon model connecting information and thermodynamics, Chin. Phys. Lett. **33**, 080501 (2016).

[35] S. Rana and A. Jayannavar, A multipurpose information engine that can go beyond the carnot limit, J. Stat. Mech.: Theory Exp. (2016) 103207.

[36] P. Strasberg, G. Schaller, T. Brandes, and C. Jarzynski, Second laws for an information driven current through a spin valve, Phys. Rev. E **90**, 062107 (2014).

[37] Y. Cao, Z. Gong, and H. T. Quan, Thermodynamics of information processing based on enzyme kinetics: An exactly solvable model of an information pump, Phys. Rev. E **91**, 062117 (2015).

[38] S. Deffner, Information-driven current in a quantum Maxwell demon, Phys. Rev. E **88**, 062128 (2013).

[39] A. Chapman and A. Miyake, How an autonomous quantum Maxwell demon can harness correlated information, Phys. Rev. E **92**, 062125 (2015).
[40] J. Stevens and S. Deffner, Quantum to classical transition in an information ratchet, Phys. Rev. E **99**, 042129 (2019).
[41] A. B. Boyd, D. Mandal, and J. P. Crutchfield, Identifying functional thermodynamics in autonomous Maxwellian ratchets, New J. Phys. **18**, 023049 (2016).
[42] A. B. Boyd, D. Mandal, and J. P. Crutchfield, Leveraging environmental correlations: The thermodynamics of requisite variety, J. Stat. Phys. **167**, 1555 (2017).
[43] A. B. Boyd, D. Mandal, P. M. Riechers, and J. P. Crutchfield, Transient Dissipation and Structural Costs of Physical Information Transduction, Phys. Rev. Lett. **118**, 220602 (2017).
[44] A. B. Boyd, D. Mandal, and J. P. Crutchfield, Correlation-powered information engines and the thermodynamics of self-correction, Phys. Rev. E **95**, 012152 (2017).
[45] A. B. Boyd, D. Mandal, and J. P. Crutchfield, Thermodynamics of Modularity: Structural Costs Beyond the Landauer Bound, Phys. Rev. X **8**, 031036 (2018).
[46] A. M. Jurgens and J. P. Crutchfield, Functional thermodynamics of Maxwellian ratchets: Constructing and deconstructing patterns, randomizing and derandomizing behaviors, Phys. Rev. Res. **2**, 033334 (2020).
[47] N. Merhav, Sequence complexity and work extraction, J. Stat. Mech.: Theory Exp. (2015) P06037.
[48] N. Merhav, J. Stat. Mech.: Theory Exp. (2017) 023207.
[49] D. H. Wolpert, The stochastic thermodynamics of computation, J. Phys. A: Math. Theor. **52**, 193001 (2019).
[50] P. Strasberg, G. Schaller, T. Brandes, and M. Esposito, Quantum and Information Thermodynamics: A Unifying Framework Based on Repeated Interactions, Phys. Rev. X **7**, 021003 (2017).
[51] R. Sánchez, P. Samuelsson, and P. P. Potts, Autonomous conversion of information to work in quantum dots, Phys. Rev. Res. **1**, 033066 (2019).
[52] N. Freitas and M. Esposito, Characterizing autonomous Maxwell demons, Phys. Rev. E **103**, 032118 (2021).
[53] J. M. Horowitz, T. Sagawa, and J. M. R. Parrondo, Imitating Chemical Motors with Optimal Information Motors, Phys. Rev. Lett. **111**, 010602 (2013).
[54] M. Bauer, A. C. Barato, and U. Seifert, Optimized finite-time information machine, J. Stat. Mech.: Theory Exp. **2014**, P09010 (2014).
[55] N. Shiraishi, T. Matsumoto, and T. Sagawa, Measurement-feedback formalism meets information reservoirs, New J. Phys. **18**, 013044 (2016).
[56] B. Annby-Andersson, P. Samuelsson, V. F. Maisi, and P. P. Potts, Maxwell's demon in a double quantum dot with continuous charge detection, Phys. Rev. B **101**, 165404 (2020).
[57] J. M. Horowitz and M. Esposito, Thermodynamics with Continuous Information Flow, Phys. Rev. X **4**, 031015 (2014).
[58] J. Schnakenberg, Network theory of microscopic and macroscopic behavior of master equation systems, Rev. Mod. Phys. **48**, 571 (1976).
[59] W. G. van der Wiel, S. De Franceschi, J. M. Elzerman, T. Fujisawa, S. Tarucha, and L. P. Kouwenhoven, Electron transport through double quantum dots, Rev. Mod. Phys. **75**, 1 (2002).
[60] R. Hanson, L. P. Kouwenhoven, J. R. Petta, S. Tarucha, and L. M. K. Vandersypen, Spins in few-electron quantum dots, Rev. Mod. Phys. **79**, 1217 (2007).
[61] M. A. Cotta, Quantum dots and their applications: What lies ahead?, ACS Appl. Nano Mater. **3**, 4920 (2020).
[62] D. V. Averin, M. Möttönen, and J. P. Pekola, Maxwell's demon based on a single-electron pump, Phys. Rev. B **84**, 245448 (2011).
[63] T. L. Hill and R. M. Simmons, Free energy levels and entropy production associated with biochemical kinetic diagrams., Proc. Natl. Acad. Sci. USA **73**, 95 (1976).
[64] T. Hill, *Free Energy Transduction and Biochemical Cycle Kinetics*, Dover Books on Chemistry (Dover Publications, Mineola, NY, 2013).
[65] C. D. Meyer, *Matrix Analysis and Applied Linear Algebra* (Siam, Philadelphia, PA, 2000), Vol. 71.
[66] B. Efron and R. Tibshirani, *An Introduction to the Bootstrap* (CRC Press, Boca Raton, FL, 1994).
[67] D. Hartich, A. C. Barato, and U. Seifert, Stochastic thermodynamics of bipartite systems: transfer entropy inequalities and a Maxwell's demon interpretation, J. Stat. Mech.: Theory Exp. (2014) P02016.
[68] G. Diana and M. Esposito, Mutual entropy production in bipartite systems, J. Stat. Mech.: Theory Exp. (2014) P04010.
[69] D. Barker, S. Lehmann, L. Namazi, M. Nilsson, C. Thelander, K. A. Dick, and V. F. Maisi, Individually addressable double quantum dots formed with nanowire polytypes and identified by epitaxial markers, Appl. Phys. Lett. **114**, 183502 (2019).
[70] D. T. Gillespie, Stochastic simulation of chemical kinetics, Annu. Rev. Phys. Chem. **58**, 35 (2007).
[71] D. T. Gillespie, A general method for numerically simulating the stochastic time evolution of coupled chemical reactions, J. Comput. Phys. **22**, 403 (1976).
[72] D. T. Gillespie, Exact stochastic simulation of coupled chemical reactions, J. Phys. Chem. **81**, 2340 (1977).